Enhanced CO2 stability of oxyanion doped Ba2In2O5 systems co-doped with La, Zr

Shin, Jaegil; Slater, Peter

DOI:
10.1016/j.jpowsour.2011.06.03
10.1016/j.jpowsour.2011.06.003

Citation for published version (Harvard):
Shin, J & Slater, P 2011, 'Enhanced CO2 stability of oxyanion doped Ba2In2O5 systems co-doped with La, Zr', Journal of Power Sources, vol. 196, no. 20, pp. 8539-8543. https://doi.org/10.1016/j.jpowsour.2011.06.03, https://doi.org/10.1016/j.jpowsour.2011.06.003

Enhanced CO_2 stability of oxyanion doped $Ba_2In_2O_5$ systems co-doped with La, Zr

J.F. Shin, P.R. Slater*

School of Chemistry, University of Birmingham, Birmingham. B15 2TT. UK

*Correspondence to

Dr. P.R. Slater
School of Chemistry
University of Birmingham
Birmingham B15 2TT
UK

p.r.slater@bham.ac.uk

Tel. +44 (0)1214148906
Fax +44 (0)1214144403

Abstract

In the Solid Oxide Fuel Cell (SOFC) field, proton conducting perovskite electrolytes offer many potential benefits. However, an issue with these electrolytes is their stability at elevated temperatures in the presence of CO_2. Recently we have reported enhanced oxide ion/proton conductivity in oxyanion (silicate, phosphate) doped $Ba_2In_2O_5$, and in this paper we extend this work to examine the stability at elevated temperatures towards CO_2. The results show improved CO_2 stability compared to the undoped system, and moreover this can be further improved by co-doping on either the Ba site with La, or the In site with Zr. While this co-doping strategy does reduce the conductivity slightly, the greatly improved CO_2 stability would suggest there is technological potential for these co-doped samples.

Keywords: Perovskite, Proton Conductivity, Solid Oxide Fuel Cell, Electrolyte, Silicon

1. Introduction

Materials displaying high proton conductivity have attracted considerable attention due to potential applications in solid oxide fuel cells, hydrogen sensors and separation membranes [1-4]. The systems showing the highest proton conductivity are the Ba containing perovskites, $BaZrO_3$ and $BaCeO_3$, suitably doped. However, a major problem with such proton conducting perovskites is the issue of stability towards CO_2. Thus, although doped $BaCeO_3$ shows excellent proton conductivity, it suffers from a distinct instability towards CO_2 at typical fuel cell operating temperatures (600-800 $^{\circ}$C), leading to the formation of $BaCO_3$. Doped $BaZrO_3$ shows much greater stability, but has been shown to suffer from poor grain boundary conductivity leading typically to significantly lower total conductivities than $BaCeO_3$ based systems. However, it should be noted that recently there have been significant improvements in the performance of $BaZrO_3$ based electrolytes through appropriate synthesis/processing to ensure the grain size is large and the samples are well sintered [5, 6].

$Ba_2In_2O_5$ has also attracted substantial interest in terms of both oxide ion conductivity and proton conductivity [7-20]. While the conductivity of the undoped material is comparatively low at intermediate temperatures, due to ordering of the oxide ion vacancies, oxide ion disorder can be introduced through doping on the In and/or Ba site, leading to a substantial enhancement in the oxide ion conductivity. In addition, both doped and undoped $Ba_2In_2O_5$ show significant proton conductivity at intermediate temperatures in a wet atmosphere. In this earlier work on $Ba_2In_2O_5$, the dopants chosen were cations with similar size e.g. La for Ba, Zr for In. Recently we have been

investigating an alternative doping strategy involving the incorporation of oxyanions. This work showed that enhanced oxide ion conductivities could be achieved by doping $Ba_2In_2O_5$ with oxyanions (phosphate, sulphate, silicate) [21-23], along with significant proton conductivities in wet atmospheres below ≈650 °C. In this paper, we extend this work to investigate the CO_2 stability of these doped samples. We also investigate the effect of co-doping on the Ba or In site with La and Zr respectively, with regards to the conductivity and the CO_2 stability.

2. Experimental

High purity $BaCO_3$, La_2O_3, In_2O_3, ZrO_2, and SiO_2, $NH_4H_2PO_4$ were used to prepare $Ba_2In_{1.8}Si_{0.2}O_{5.1}$, $Ba_2In_{1.7}P_{0.3}O_{5.3}$ and La, Zr co-doped samples. In order to overcome Ba loss at elevated temperatures, a 3% excess of $BaCO_3$ was employed. Without this small Ba excess, low levels of Ba deficient impurity phases, such as $BaIn_2O_4$ and $Ba_4In_6O_{13}$, were observed after sintering, as has been seen in other studies synthesising similar Ba containing phases [24,25]. The powders were intimately ground and heated initially to 1000 °C for 12h, before dry-milling (350 rpm for 1 hour, Fritsch Pulverisette 7 Planetary Ball Mill) and reheating to 1000 °C for a further 50h. The resulting powders were then pressed as pellets (1.3 cm diameter) and sintered at 1400 °C for 10h. In order to limit the amount of Ba loss during the sintering process, the pellets were covered in sample powder and the crucible was covered with a lid. Phase purity was determined using X-ray powder diffraction (Bruker D8 diffractometer with Cu $K\alpha_1$ radiation).

In order to determine the CO_2 stability of samples, two sets of experiments were performed. In the first set of experiments, samples were heated at temperatures between 600 and 800 $^{\circ}$C for 12 hours in a tube furnace under flowing CO_2 gas, and the samples were analysed for partial decomposition by X-ray diffraction. In the second experiment samples were analysed using thermogravimetric analysis (Netzsch STA 449 F1 Jupiter Thermal Analyser). Samples were heated at 10 $^{\circ}$C min^{-1} to 1000 $^{\circ}$C in 1:1 CO_2 and N_2 mixture to determine at what temperature CO_2 pick up occurred.

For the conductivity measurements a Norecs Probostat^{TM} measurement cell was employed [26, 27]. The sintered pellets (>85% theoretical density) were coated with Pt paste, and then heated to 800 °C for 1 hour to ensure bonding to the pellet. Conductivities were then measured by AC impedance measurements (Hewlett Packard 4182A impedance analyser) in the range from 0.1 to 10^3 kHz, with an applied voltage of 100 mV. Since $Ba_2In_2O_5$ displays a small p-type contribution to the conductivity in oxidising conditions, measurements were made in dry N_2 to eliminate this contribution. In addition, measurements were made in wet N_2 (in which the gas was bubbled at room temperature through water) to identify any protonic contribution to the conductivity. The impedance data for the P, Si singly doped and La/P, La/Si co-doped samples showed a single broad semicircle in both dry and wet atmospheres (figure 1). The capacitance of the semicircle ($\approx 10^{-12}$ Fcm^{-1}) was typical of a bulk response, suggesting that the resistance of the grain boundary was small compared to that of the bulk. For the Zr/Si and Zr/P co-doped samples, a single semicircle was observed above 400 $^{\circ}$C, while below this temperature a small grain boundary component was also observed. The conductivities reported represent total conductivities.

3. Results and discussion

As shown in our previous work, X-ray powder diffraction analysis indicated that on Si, P doping there is a change in symmetry from orthorhombic for $Ba_2In_2O_5$ to cubic for $Ba_2In_{1.8}Si_{0.2}O_{5.1}$, and $Ba_2In_{1.7}P_{0.3}O_{5.3}$ [21-23]. The stability of these systems towards CO_2 was examined by heating in CO_2 at different temperatures between 600 and 800 $^{\circ}$C, and through TGA studies in a 1:1 N_2:CO_2 atmosphere between 10 and 1000 $^{\circ}$C. The results showed that on heating to 600°C, $BaCO_3$ impurities were visible for all samples (figure 2). However, compared to undoped $Ba_2In_2O_5$, the Si, P doped samples showed significantly lower sensitivity towards CO_2, with much smaller $BaCO_3$ impurities observed at this temperature. The results were also compared to Y doped $BaCeO_3$ which is known to be very sensitive towards CO_2. As for undoped $Ba_2In_2O_5$, this phase showed the presence of large $BaCO_3$ impurities when heated in CO_2 at 600 $^{\circ}$C. The TGA results provided further indication of the relative stabilities of the samples towards CO_2 (figure 3). For undoped $Ba_2In_2O_5$ a clear increase in mass, consistent with CO_2 pick up and formation of $BaCO_3$, was observed at 600 $^{\circ}$C. Similarly, for $BaCe_{0.9}Y_{0.1}O_{2.95}$ a significant increase in mass was observed above 500 $^{\circ}$C. In contrast, for phosphate and silicate doped $Ba_2In_2O_5$, the TGA traces were much flatter, with a large mass increase only observed when the temperature was raised further to above 800 $^{\circ}$C.

These initial results therefore indicated that the stability of $Ba_2In_2O_5$ towards CO_2 was improved by silicate or phosphate doping, although the samples still showed some instability at higher temperatures. Therefore, the effect of co-doping with La, Zr was examined to determine the effect on both the CO_2 stability and conductivity. Single phase

$Ba_{2-x}La_xIn_{1.7}P_{0.3}O_{5.3+x/2}$, $Ba_{2-x}La_xIn_{1.8}Si_{0.2}O_{5.1+x/2}$ ($0 \leq x \leq 0.4$) and $Ba_2In_{1.7-x}Zr_xP_{0.3}O_{5.3+x/2}$, $Ba_2In_{1.8-x}Zr_xSi_{0.2}O_{5.1+x/2}$ ($0 \leq x \leq 0.4$) were prepared, and the CO_2 stability and conductivities were examined. The preliminary studies showed that as the La, Zr content increased, so the stability towards CO_2 appeared to increase, although this was at the expense of a general reduction in the conductivity. Thus, La, Zr co-doping appears beneficial in terms of the CO_2 stability but detrimental in terms of the conductivity. In terms of a balance between high conductivity and CO_2 stability, the compositions $Ba_{1.7}La_{0.3}In_{1.7}P_{0.3}O_{5.45}$, $Ba_2In_{1.5}Zr_{0.2}P_{0.3}O_{5.4}$, $Ba_{1.6}La_{0.4}In_{1.8}Si_{0.2}O_{5.3}$, $Ba_2In_{1.6}Zr_{0.2}Si_{0.2}O_{5.2}$ were identified as the most promising, and so these compositions were analysed in more detail. XRD patterns for these samples are shown in figure 4, with their cell parameters and those for undoped $Ba_2In_2O_5$ and singly Si/P doped samples given in table 1. These data show a decrease in cell volume on Zr, La incorporation consistent with the smaller size of Zr^{4+}, La^{3+} compared to In^{3+}, Ba^{2+} respectively, with the larger difference between the sizes of La^{3+} and Ba^{2+} leading to a greater decrease in cell volume for La doping.

The conductivities of these co-doped samples are shown in figure 5, and a comparison with those of singly doped $Ba_2In_{1.7}P_{0.3}O_{5.3}$ and $Ba_2In_{1.8}Si_{0.2}O_{5.1}$ shown in table 2. As can be seen from these data, the Si doped samples show the highest conductivities, and Zr co-doping appears to show a lower decrease than for La co-doping. This may reflect the larger cell size for the former Zr doped samples. Overall the conductivities show high values, with a significant enhancement below ≈650 $^{\circ}$C in wet atmospheres due to proton conductivity. For $Ba_2In_{1.6}Zr_{0.2}Si_{0.2}O_{5.2}$ a conductivity of 2.7 x 10^{-3} Scm^{-1} at 500 $^{\circ}$C was observed in wet N_2, which represents a promising value for technological applications.

Measurements of the CO_2 stability of these four co-doped samples showed no evidence by X-ray diffraction for any $BaCO_3$ formation on heating in CO_2 at 600 $^{\circ}$C, where small $BaCO_3$ impurities were seen for the singly doped samples. Further studies were performed at higher temperatures up to 800 $^{\circ}$C. These studies showed the presence of small $BaCO_3$ impurities for the Zr/P and La/P co-doped systems at 800 $^{\circ}$C, while for the Si/Zr and La/Si co-doped materials, no $BaCO_3$ was visible, highlighting the excellent CO_2 stability of these latter phases (figure 6). The TGA studies in a 1:1 CO_2:N_2 atmosphere also showed no significant mass change for the Zr/Si and La/Si co-doped systems, although expanding the scale of the data showed that there was a small mass increase for the Zr/P and La/P co-doped systems above 600 $^{\circ}$C (figure 7). Overall the results therefore showed improved CO_2 stability for these co-doped systems, especially for the La/Si and Zr/Si co-doped samples.

The origin of the enhancement in CO_2 stability can be attributed to two factors, as illustrated by work by Yi *et al.* on the stability of Ba(Fe,Co, Nb)O_{3-x} perovskite cathode materials [28]. In this work the authors showed that improved stability of the perovskite towards CO_2 could be attributed to reduced oxide ion vacancy levels and increased acidity of the perovskite. In the present study, the incorporation of phosphate, silicate, zirconium and lanthanum will increase the oxygen content, and hence reduce the number of oxide ion vacancies. This reduction in oxide ion vacancies may be partly responsible, however, for the observed reduction in conductivity on co-doping with Si/P and La/Zr. All the dopants are also likely to increase the acidity of the system, although it might be expected from this that the phosphate doped system would be more stable due to both the

higher acidity and higher oxygen content. In contrast, the Si doped systems proved the most stable, and the origin of this improved stability requires further investigation.

4. Conclusions

The results show that phosphate or silicate doping into $Ba_2In_2O_5$ leads to an improvement in the stability towards CO_2. Furthermore, co-doping with La or Zr leads to even greater stability, with the composition $Ba_2In_{1.6}Zr_{0.2}Si_{0.2}O_{5.2}$ showing particularly promise, due to the high conductivity and high stability.

Acknowledgements

We would like to express thanks to the University of Birmingham for funding (EPS international studentship for JFS).

The Bruker D8 diffractometer, and Netzsch thermal analyser used in this research were obtained through the Science City Advanced Materials project: Creating and Characterising Next generation Advanced Materials project, with support from Advantage West Midlands (AWM) and part funded by the European Regional Development Fund (ERDF).

The funding agencies had no involvement in the collection, analysis and interpretation of data; in the writing of the report; and in the decision to submit the paper for publication.

References

1. T. Norby, Y. Larring, Current Opinion in Solid State and Materials Science 2 (1997**)** 593.

2. K.D. Kreuer, Annu. Rev. Mater. Res., 33 (2003) 333.
3. L. Malavasi, C.A.J. Fisher, M.S. Islam, J. Mater. Chem. 39 (2010**)** 4370.
4. A. Orera, P.R. Slater, Chem. Mater. 22 (2010) 675.
5. P. Babilo, S.M. Haile, J. Am. Ceram. Soc. 88 (2005) 2362.
6. S.W. Tao, J.T.S. Irvine, J. Solid State Chem. 180 (2007) 3493.
7. J.B. Goodenough, J.E. Ruizdiaz, Y.S. Zhen, Solid State Ionics 44 (1990) 21.
8. S.A. Speakman, J.W. Richardson, B.J. Mitchell, S.T. Misture, Solid State Ionics 149 (2002) 247.
9. T. Schober, Solid State Ionics 109 (1998**)** 1.
10. V. Jayaraman, A. Magrez, M. Caldes, O. Joubert, M. Ganne, Y. Piffard, L. Brohan, Solid State Ionics 170 (2004) 17.
11. A. Rolle, R.N. Vannier, N.V. Giridharan, F. Abraham, Solid State Ionics 176 (2005) 2095.
12. T. Schrober, J. Friedrich, Solid State Ionics 113 (1998) 369.
13. G.B. Zhang, D.M. Smith, Solid State Ionics 82 (1995) 153.
14. E. Quarez, S. Noirault, M.T. Caldes, O. Joubert, J. Power Sources 195 (2010) 1136.
15. M. Karlsson, A. Matic, C.S. Knee, I. Ahmed, S.G. Eriksson, L. Borjesson, Chem. Mater. 20 (2008) 3480.
16. F. Giannici, A. Longo, A. Balerna, K.D. Kreuer, A. Martorana, Chem. Mater. 19 (2010) 5714.
17. S. Noirault, S. Celerier, O. Joubert, M.T. Caldes, Y. Piffard, Solid State Ionics 178 (2007) 1353.

18. I. Ahmed, S.G. Eriksson, E. Ahlberg, C.S. Knee, P. Berastegui, L.G. Johansson, H. Rundlof, M. Karlsson, A. Matic, L. Borjesson, D. Engberg, Solid State Ionics 177 (2006) 1395.
19. K. Kakinuma, A. Tomita, H. Yamamura, T. Atake, J. Mater. Sci. 41 (2006) 6435.
20. C.A.J. Fisher, M.S. Islam, Solid State Ionics 118 (1999) 355.
21. J.F. Shin, L. Hussey, A. Orera, P.R. Slater, Chem. Commun. 46 (2010**)** 4613.
22. J.F. Shin, A. Orera, D.C. Apperley, P.R. Slater, J. Mater. Chem. 21 (2011) 874.
23. J.F. Shin, D.C. Apperley, P.R. Slater, Chem. Mater. 22 (2010) 5945.
24. T. Omata, T. Fuke, S. Otsuka-Yao-Matsuo, Solid State Ionics 177 (2006) 2447.
25. A.M. Abakumov, M.D. Rossell, O.Y. Gutnikova, O.A. Drozhzhin, L.S. Leonova, Y.A. Dobrovolsky, S.Y. Istomin, G. Van Tendeloo, E.V. Antipov, Chem. Mater. 20 (2008) 4457
26. www.norecs.com
27. R. Haugsrud, Y. Larring, T. Norby; Solid State Ionics 176 (2005) 2957.
28. J.X. Yi, M. Schroeder, T. Weirich, J. Maier, Chem. Mater. 22 (2010) 6246.

Figure Captions

Fig. 1 Fitted impedance data for $Ba_{1.6}La_{0.4}In_{1.8}Si_{0.2}O_{5.3}$ at 310 °C: dry N_2 (square) and wet N_2 (cross).

Fig. 2 XRD patterns for (a) $Ba_2In_{1.8}Si_{0.2}O_{5.1}$, (b) $Ba_2In_{1.7}P_{0.3}O_{5.3}$, (c) $Ba_2In_2O_5$ and (d) $Ba_2Ce_{0.9}Y_{0.1}O_{2.95}$ after heating in CO_2 at 600 °C for 12h (main $BaCO_3$ impurity peaks marked *)

Fig. 3 TG profiles (10 °C min^{-1} to 1000 °C in 1:1 CO_2 and N_2 mixture) for (a) $Ba_2In_2O_5$, (b) $Ba_2Ce_{0.9}Y_{0.1}O_{2.95}$, (c) $Ba_2In_{1.7}P_{0.3}O_{5.3}$ and (d) $Ba_2In_{1.8}Si_{0.2}O_{5.1}$.

Fig. 4 XRD patterns of (a) $Ba_{1.7}La_{0.3}In_{1.7}P_{0.3}O_{5.45,}$ (b) $Ba_2In_{1.5}Zr_{0.2}P_{0.3}O_{5.4}$, (c) $Ba_{1.6}La_{0.4}In_{1.8}Si_{0.2}O_{5.3}$ and (d) $Ba_2In_{1.6}Zr_{0.2}Si_{0.2}O_{5.2}$ showing single phase cubic perovskite systems.

Fig. 5(a) Conductivity data for $Ba_{1.7}La_{0.3}In_{1.7}P_{0.3}O_{5.45}$ in dry N_2 (filled square) and wet N_2 (open square) and for $Ba_2In_{1.5}Zr_{0.2}P_{0.3}O_{5.4}$ in dry N_2 (filled circle) and wet N_2 (open circle).

Fig. 5(b) Conductivity data for $Ba_{1.6}La_{0.4}In_{1.8}Si_{0.2}O_{5.3}$ in dry N_2 (filled square) and wet N_2 (open square) and for $Ba_2In_{1.6}Zr_{0.2}Si_{0.2}O_{5.2}$ in dry N_2 (filled circle) and wet N_2 (open circle).

Fig. 6 XRD patterns for (a) $Ba_{1.7}La_{0.3}In_{1.7}P_{0.3}O_{5.45,}$ (b) $Ba_2In_{1.5}Zr_{0.2}P_{0.3}O_{5.4}$, (c) $Ba_{1.6}La_{0.4}In_{1.8}Si_{0.2}O_{5.3}$ and (d) $Ba_2In_{1.6}Zr_{0.2}Si_{0.2}O_{5.2}$ after heating in CO_2 at 800 °C for12h (main $BaCO_3$ impurity peaks marked *)

Fig. 7 TG profiles (10 °C min^{-1} to 1000 °C in 1:1 CO_2 and N_2 mixture) for (a) $Ba_{1.7}La_{0.3}In_{1.7}P_{0.3}O_{5.45,}$ (b) $Ba_2In_{1.5}Zr_{0.2}P_{0.3}O_{5.4}$, (c) $Ba_2In_{1.6}Zr_{0.2}Si_{0.2}O_{5.2}$ (d)

$Ba_{1.6}La_{0.4}In_{1.8}Si_{0.2}O_{5.3}$ and (e) $Ba_2In_2O_5$.(inset: expanded scale for (a)-(d))

Table 1a Cell parameter data for P doped $Ba_2In_2O_5$ (data for the undoped and singly doped samples from ref [22])

Sample (nominal composition)	Unit cell parameters (Å)			Unit cell volume (Å^3)
	a	b	c	
$Ba_2In_2O_5$	6.089(2)	16.736(8)	5.963(2)	607.6(2)
$Ba_2In_{1.7}P_{0.3}O_{5.3}$	4.208(1)	-	-	74.5(1)
$Ba_{1.7}La_{0.3}In_{1.7}P_{0.3}O_{5.45}$	4.183(1)	-	-	73.2(1)
$Ba_2In_{1.5}Zr_{0.2}P_{0.3}O_{5.4}$	4.199(1)	-	-	74.0(1)

Table 1b Cell parameter data for Si doped $Ba_2In_2O_5$ (data for the undoped and singly doped samples from ref [23])

Sample (nominal composition)	Unit cell parameters (Å)			Unit cell volume (Å^3)
	a	b	c	
$Ba_2In_2O_5$	6.089(2)	16.736(8)	5.963(2)	607.6(2)
$Ba_2In_{1.8}Si_{0.2}O_{5.1}$	4.209(1)			74.6(1)
$Ba_{1.6}La_{0.4}In_{1.8}Si_{0.2}O_{5.3}$	4.167(1)			72.4(1)
$Ba_2In_{1.6}Zr_{0.2}Si_{0.2}O_{5.2}$	4.200(1)			74.1(1)

Table 2a. Conductivity data for P doped series (conductivity enhancement in wet atmospheres was only observed below ≈650 °C)

Sample (nominal composition)	Conductivity (S cm^{-1})		
	500 °C		800 °C
	Wet	Dry	
$Ba_2In_{1.7}P_{0.3}O_{5.3}$	1.9×10^{-3}	5.0×10^{-4}	1.2×10^{-2}
$Ba_{1.7}La_{0.3}In_{1.7}P_{0.3}O_{5.45}$	4.4×10^{-4}	1.8×10^{-4}	6.0×10^{-3}
$Ba_2In_{1.5}Zr_{0.2}P_{0.3}O_{5.4}$	9.7×10^{-4}	4.0×10^{-4}	5.3×10^{-3}

Table 2b. Conductivity data for Si doped series (conductivity enhancement in wet atmospheres was only observed below ≈650 °C)

Sample (nominal composition)	Conductivity (S cm^{-1})		
	500 °C		800 °C
	Wet	Dry	
$Ba_2In_{1.8}Si_{0.2}O_{5.1}$	4.5×10^{-3}	1.7×10^{-3}	4.3×10^{-2}
$Ba_{1.6}La_{0.4}In_{1.8}Si_{0.2}O_{5.3}$	7.7×10^{-4}	5.3×10^{-4}	1.8×10^{-2}
$Ba_2In_{1.6}Zr_{0.2}Si_{0.2}O_{5.2}$	2.7×10^{-3}	9.9×10^{-4}	2.3×10^{-2}

Fig 1

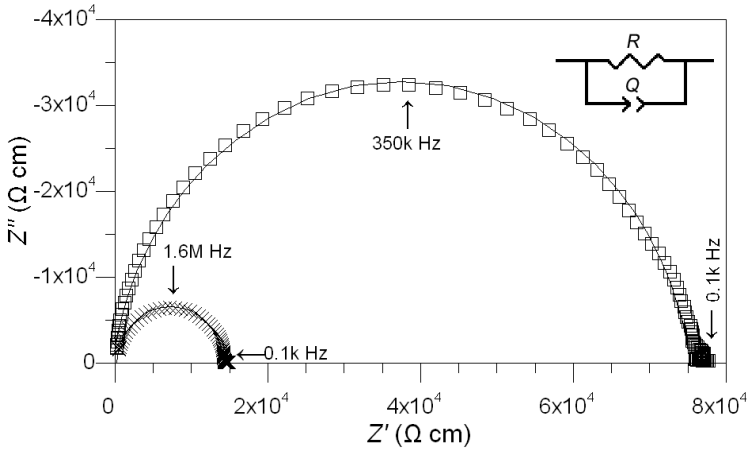
-4x10^4
-3x10^4
-2x10^4
-1x10^4
0
Z'' (Ω cm)
R
Q
350k Hz
1.6M Hz
0.1k Hz
0.1k Hz
0
2x10^4
4x10^4
6x10^4
8x10^4
Z' (Ω cm)

Fig 2

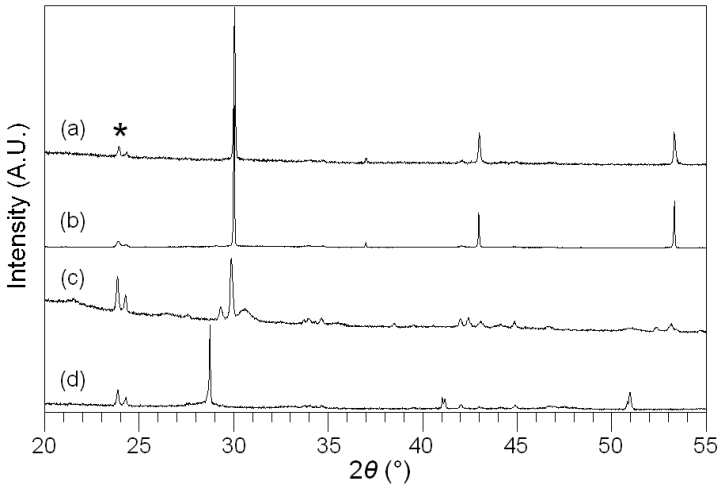

Fig. 3

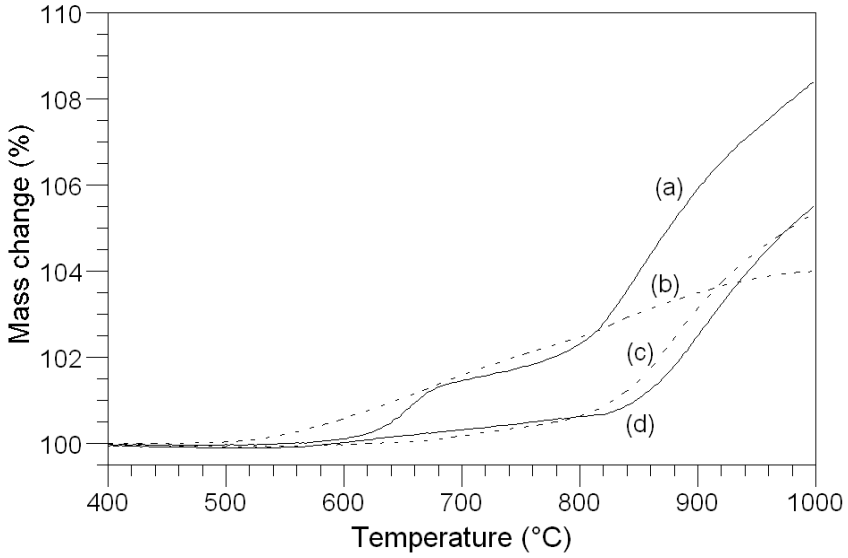
110
108
106
104
102
100
Mass change (%)
400
500
600
700
800
900
1000
Temperature (°C)
(a)
(b)
(c)
(d)

Fig 4

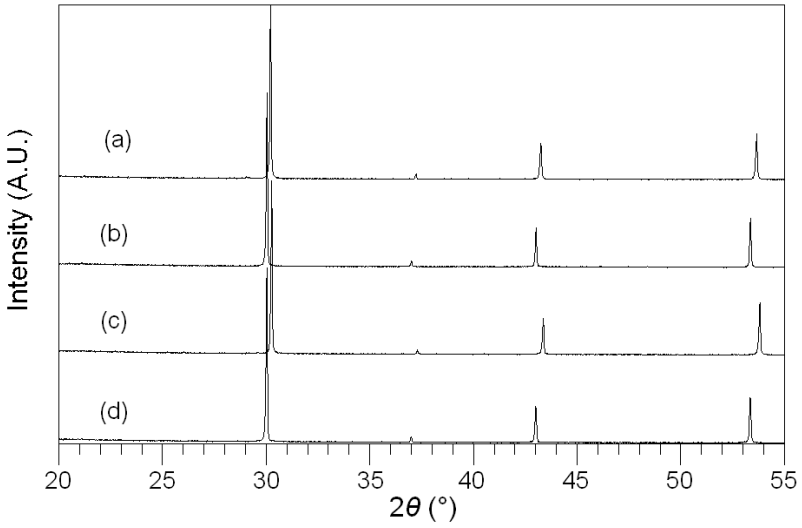

Fig 5(a)

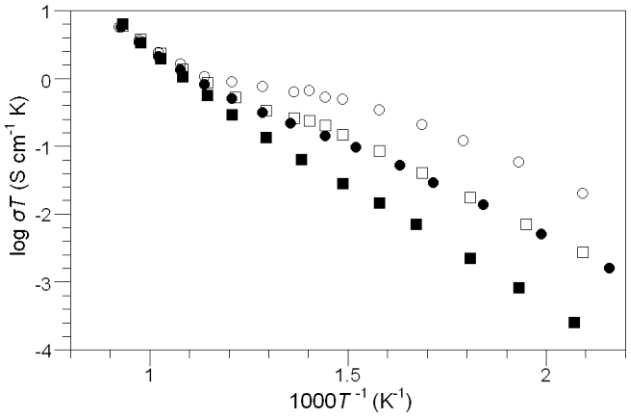
log σT (S cm-1 K)
1000T-1 (K-1)
1
0
-1
-2
-3
-4
1
1.5
2

Fig 5 (b)

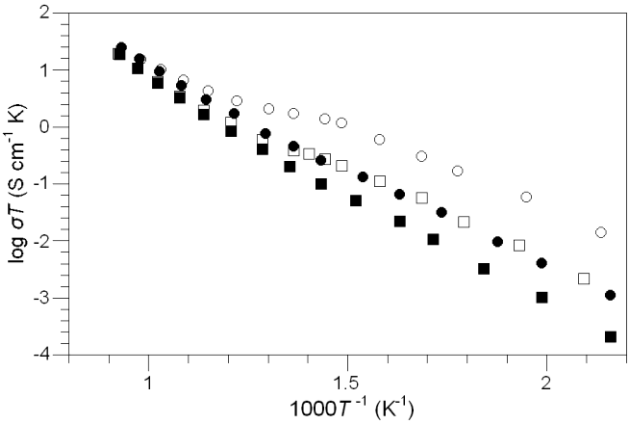
log σT (S cm-1 K)
1000T-1 (K-1)
2
1
0
-1
-2
-3
-4
1
1.5
2

Fig 6

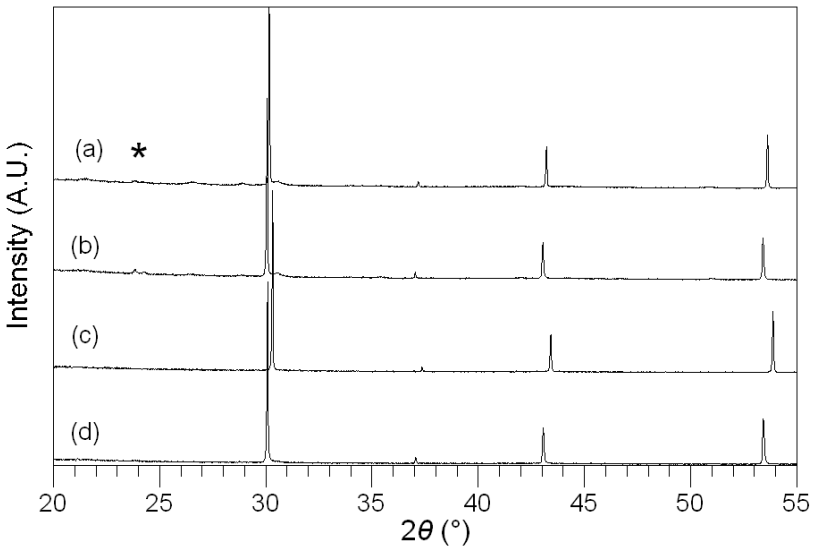

Fig 7